Source Physics Experiment at the Nevada National Security Site

SAND2020-10228PE

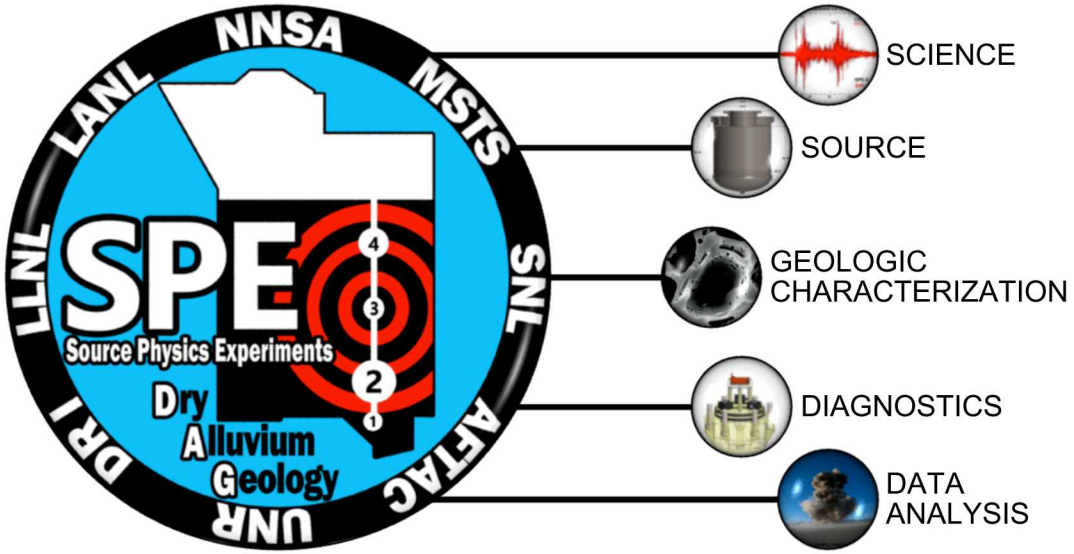

Source Physics Experiment: Dry Alluvium Geology (DAG) Gradiometric Analysis

SeismoTea 2020/10/9
Daniel Wells – University of Utah
Christian Poppeliers – Sandia National Labs

Unclassified: Unlimited Release

Sandia National Laboratories is a multimission laboratory managed and operated by National Technology & Engineering Solutions of Sandia, LLC, a wholly owned subsidiary of Honeywell International Inc., for the U.S. Department of Energy's National Nuclear Security Administration under contract DE-NA0003525.

Acknowledgments

This work was funded by the National Nuclear Security Administration, Defense Nuclear Nonproliferation Research and Development (DNN R&D), and the Source Physics Experiment (SPE) working group, a multi-institutional and interdisciplinary group of scientists and engineers. Sandia National Laboratories is a multimission laboratory managed and operated by National Technology and Engineering Solutions of Sandia Limited Liability Corporation, a wholly owned subsidiary of Honeywell International, Inc., for the U.S. Department of Energy's National Nuclear Security Administration under Contract Number DE-NA0003525. This article describes objective technical results and analysis. Any subjective views or opinions that might be expressed in the article do not necessarily represent the views of the U.S. Department of Energy or the United States government.

Introduction

- Nevada National Security Site
- Source Physics Experiment (SPE)
- Phase I in granite, Phase II in dry alluvium geology
- Underground chemical explosion source
- Goal here: investigate scattering and path effects between two different receivers from the same source using gradiometric analysis

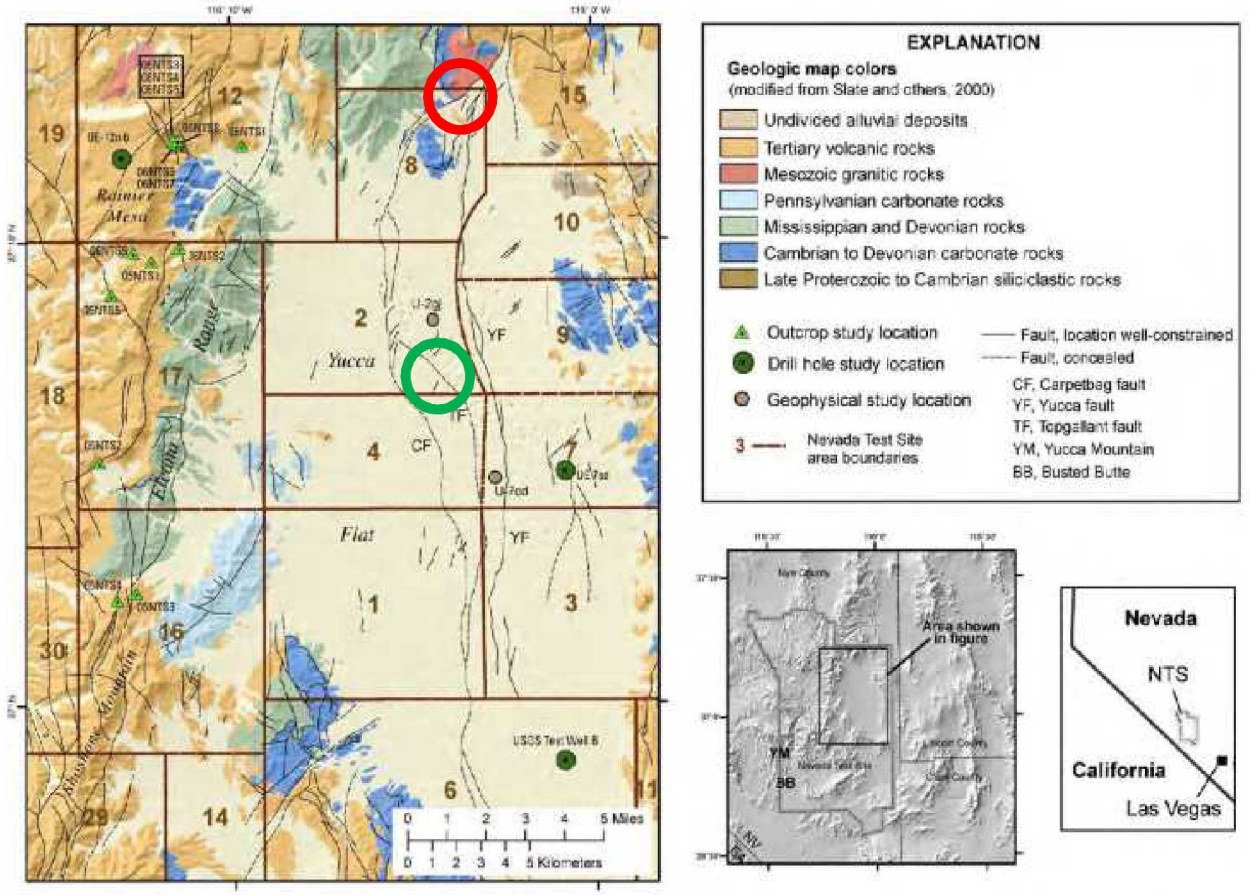

Source: Sweetkind et al, 2007

Data

Location of Dry Alluvium Geology (DAG) underground explosions and the two gradiometric arrays: GAE (gradiometer array east) and GAN (gradiometer array north). The gradiometers were 1.5 km away and roughly due east and due north, respectively, of the explosions. The ground is visibly cratered on the surface from previous explosion testing in the area. Imagery courtesy of Google.

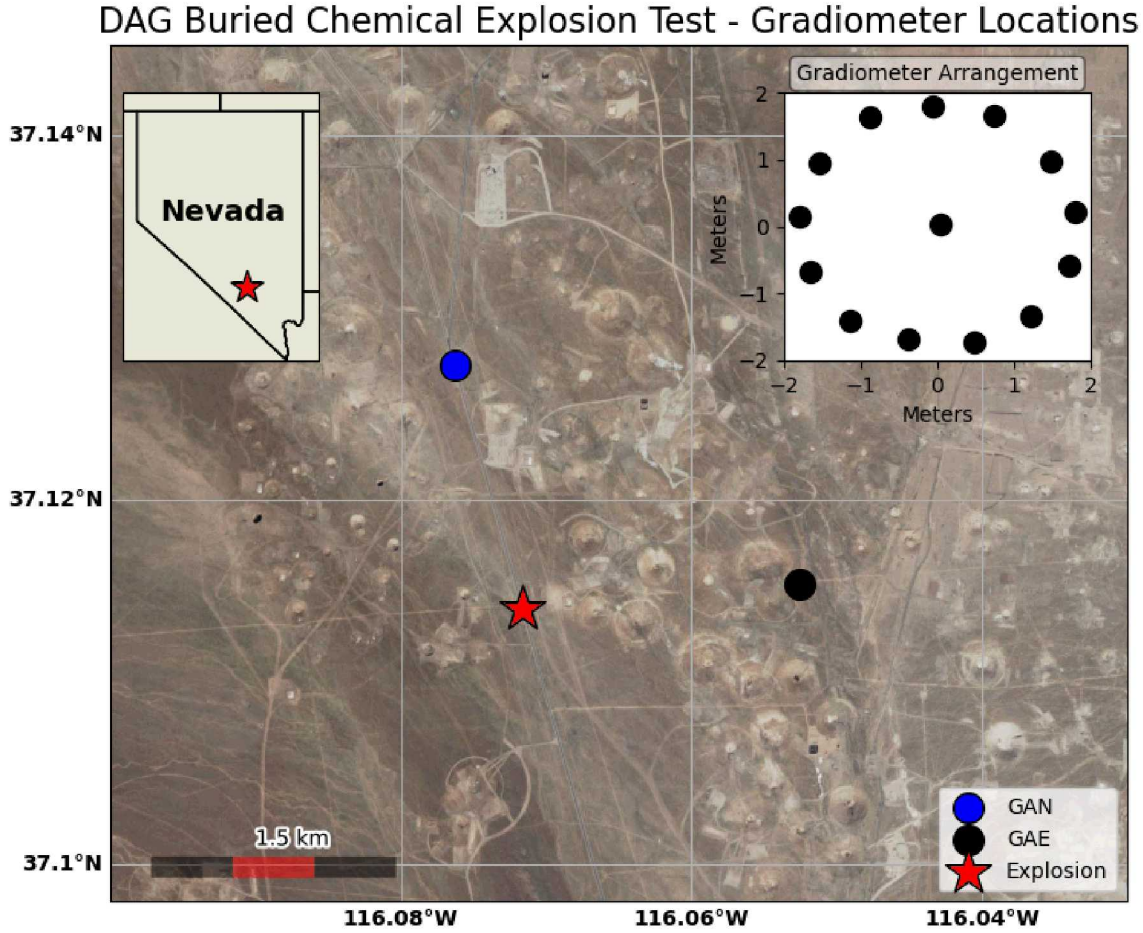

Gradiometry

- Very small, dense seismic array
- Array aperture < .1*seismic wavelength
- Spatial derivatives of seismograms averaged over array aperture
- Can use spatial gradients to compute rotational motions, $\omega_r, \omega_t, \omega_z$

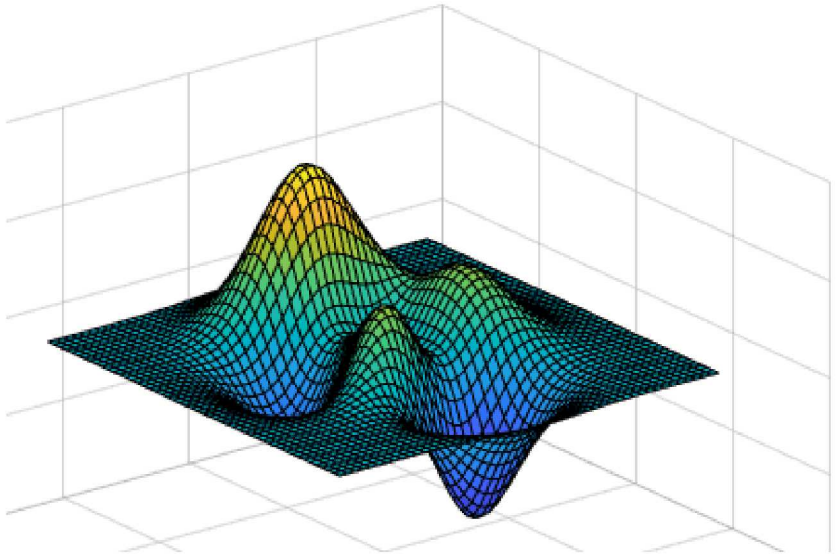

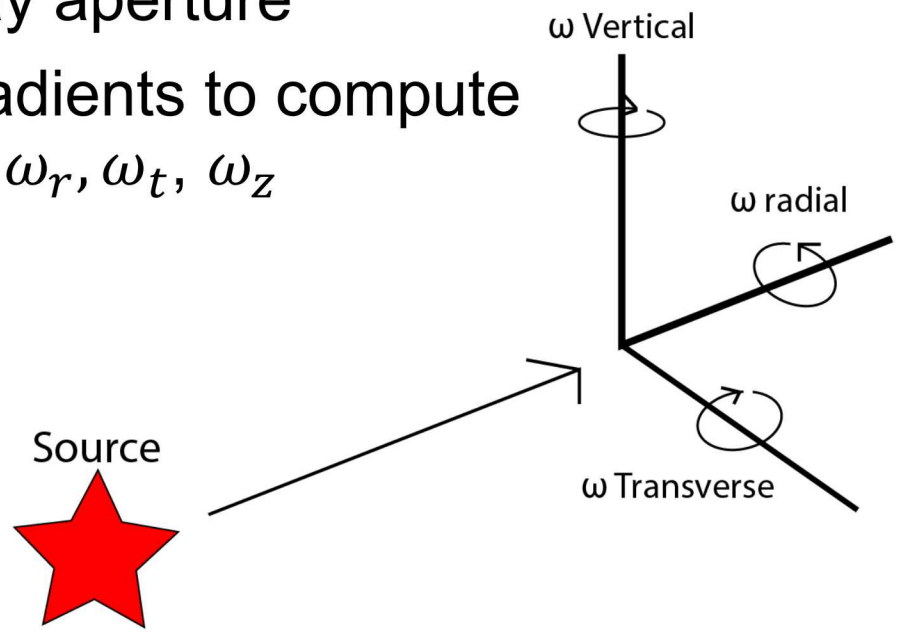

Wavelet Analysis

- **Wavelet transform** – time-frequency decomposition of a time series
- **Wavelet coherence** – compare wavelet transforms of GAE vs GAN gradiometers
- Apply methods to displacement seismograms and gradiometric wave attributes

$$C(a,b;f(t),\psi(t)) = \int_{-\infty}^{\infty} f(t)\,\frac{1}{a}\psi^*\left(\frac{t-b}{a}\right)dt$$

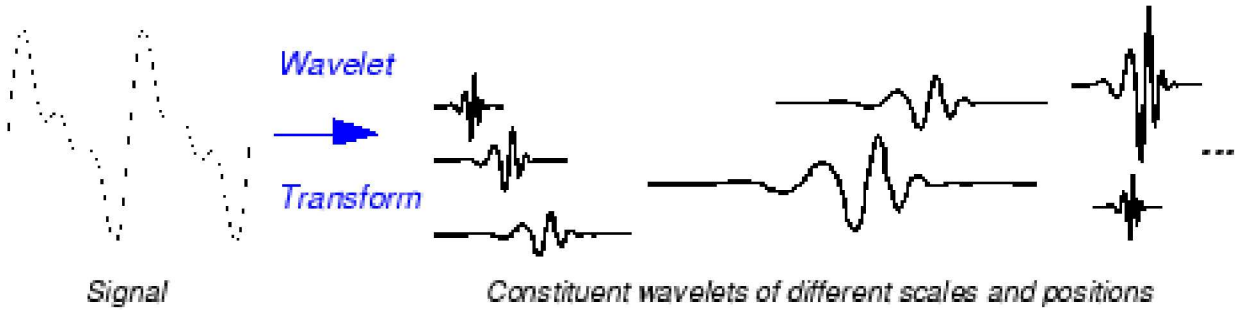

Source: Mathworks.com/help/wavelet

Wavelet Transform

- Wavelet can be translated in time and frequency
  - Stretched (translated in frequency)
  - Translated (translated in time)
- We use a complex Morlet wavelet
  - Reasonable resolution in time and frequency domain
  - Allows recovery of phase information

$$C(a,b;f(t),\psi(t)) = \int_{-\infty}^{\infty} f(t)\,\frac{1}{a}\psi^*\left(\frac{t-b}{a}\right)dt$$

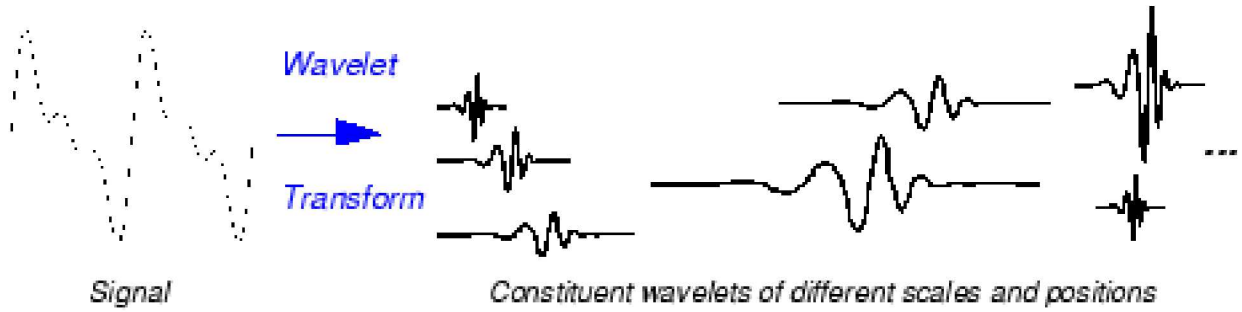

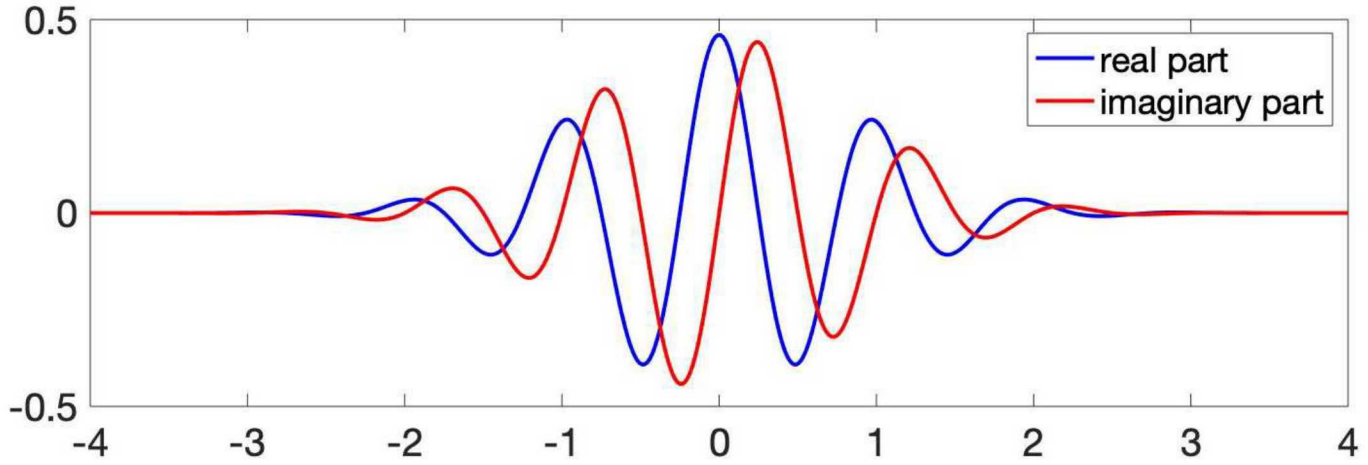

Wavelet Coherence

- Use Cross-wavelet transform (1)
  - Wavelet transform of one time series with complex conjugate of wavelet transform of 2nd series
- Wavelet coherence measures where the two series are similar (2)
  - Cross correlation between time series as a function of time and frequency
  - Complex wavelet recovers relative phase

$$W_n^{XY}(s) = W_n^X(\mathrm{s})\, W_n^{Y*}(\mathrm{s}) \quad (1)$$

$$R_n^S(s) = \frac{\left|S\left(s^{-1}W_n^{XY}(s)\right)\right|^2}{S\left(s^{-1}\left|W_n^X(s)\right|^2\right)S\left(s^{-1}\left|W_n^Y(s)\right|^2\right)} \quad (2)$$

Source: Mathworks.com/help/wavelet

Significance levels

- We follow Grinsted et al, 2004, to calculate significance levels relative to red noise
- Red noise has higher relative energy in lower frequencies
- 95% confidence level that the signal in the wavelet plots is NOT noise is outlined in plots

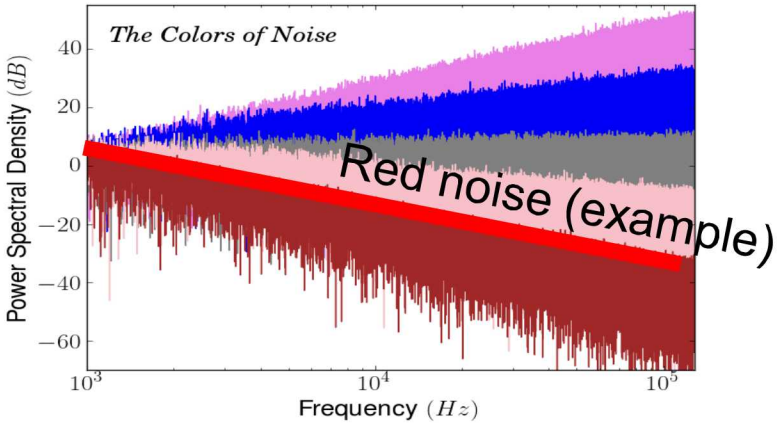

Source: Cnoise, Wikipedia/wiki/colors_of_noise

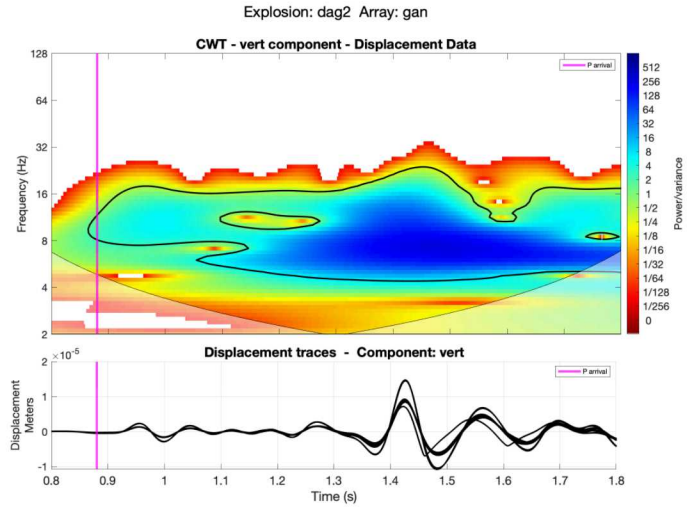

What do we expect?

- If there is appreciable scattering differences between the source and the two gradiometers, we expect low coherence for displacement data and rotation data
  - One path is very broken up from previous underground testing
  - Vertical rotation should capture much of the effect of scattering
  - Might see low coherence for radial and transverse rotation – not studied extensively
- Some frequency bands might be consistently more coherent than others
- Each explosion had a different yield and depth
  - Different coherence patterns between explosions
  - Help illuminate how travel path and scattering can affect wavefield

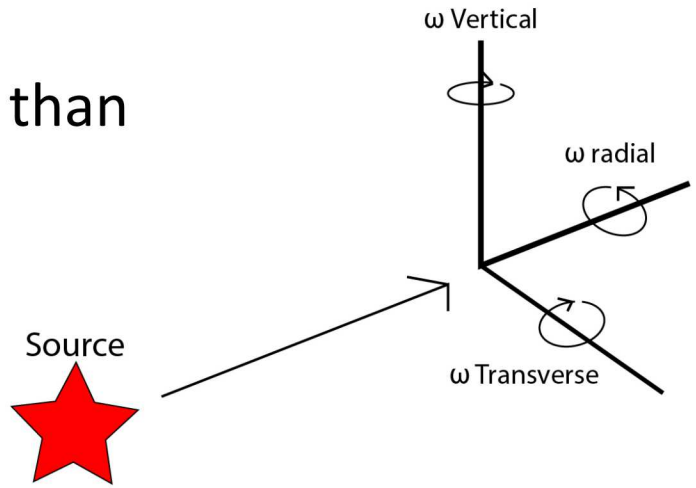

Example – Continuous Wavelet Transform

- Decomposes the signal into frequency spectrum as a function of time

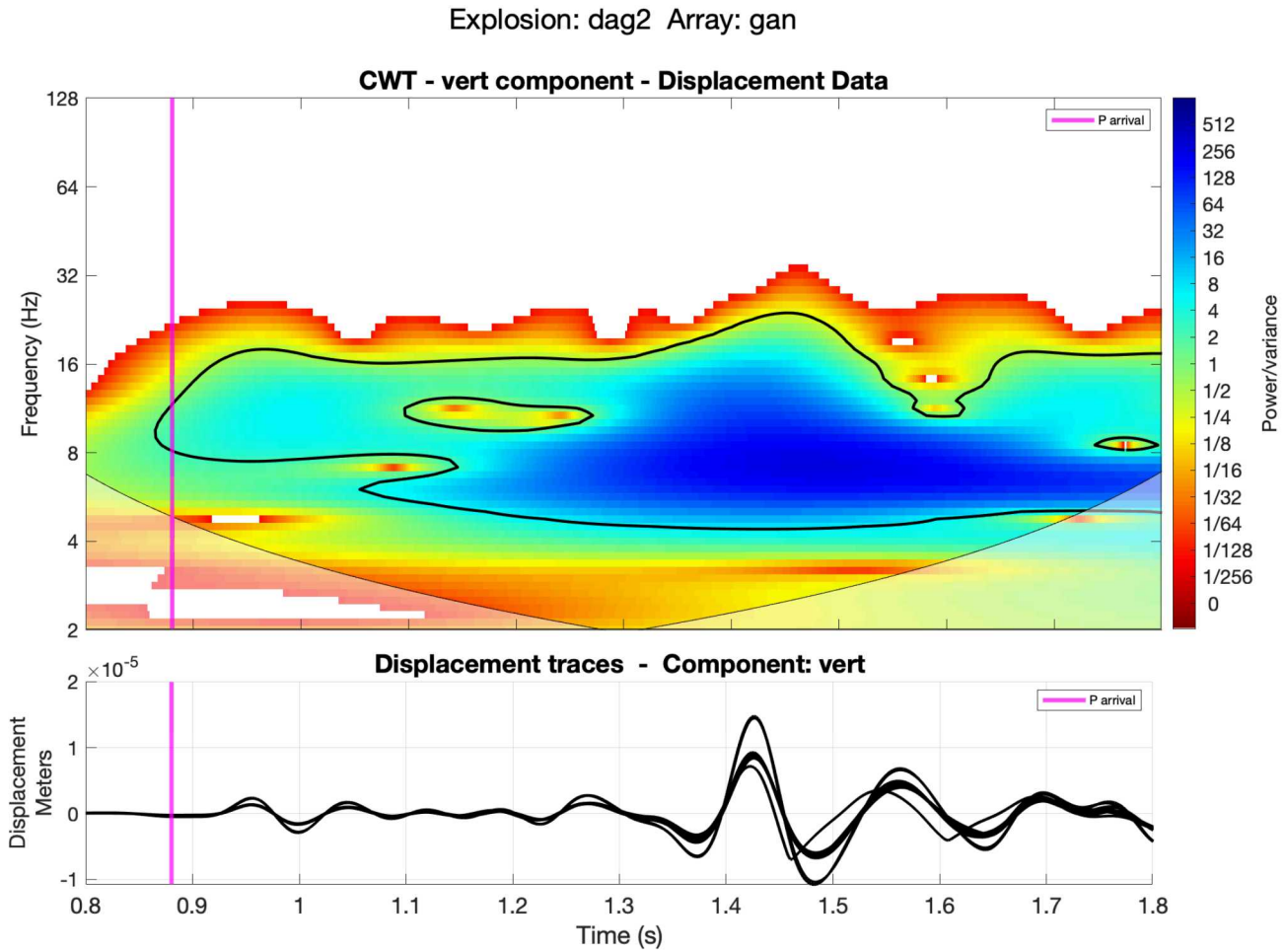

DAG 1 GAE gradiometer

Vertical component

In order from top to bottom:

1) Raw seismograms
2) Slowness in x and y direction
3) Slowness magnitude
4) Velocity magnitude
5) Azimuth of wave propagation (degrees from north)
6) Changes in radiation pattern, in x and y direction

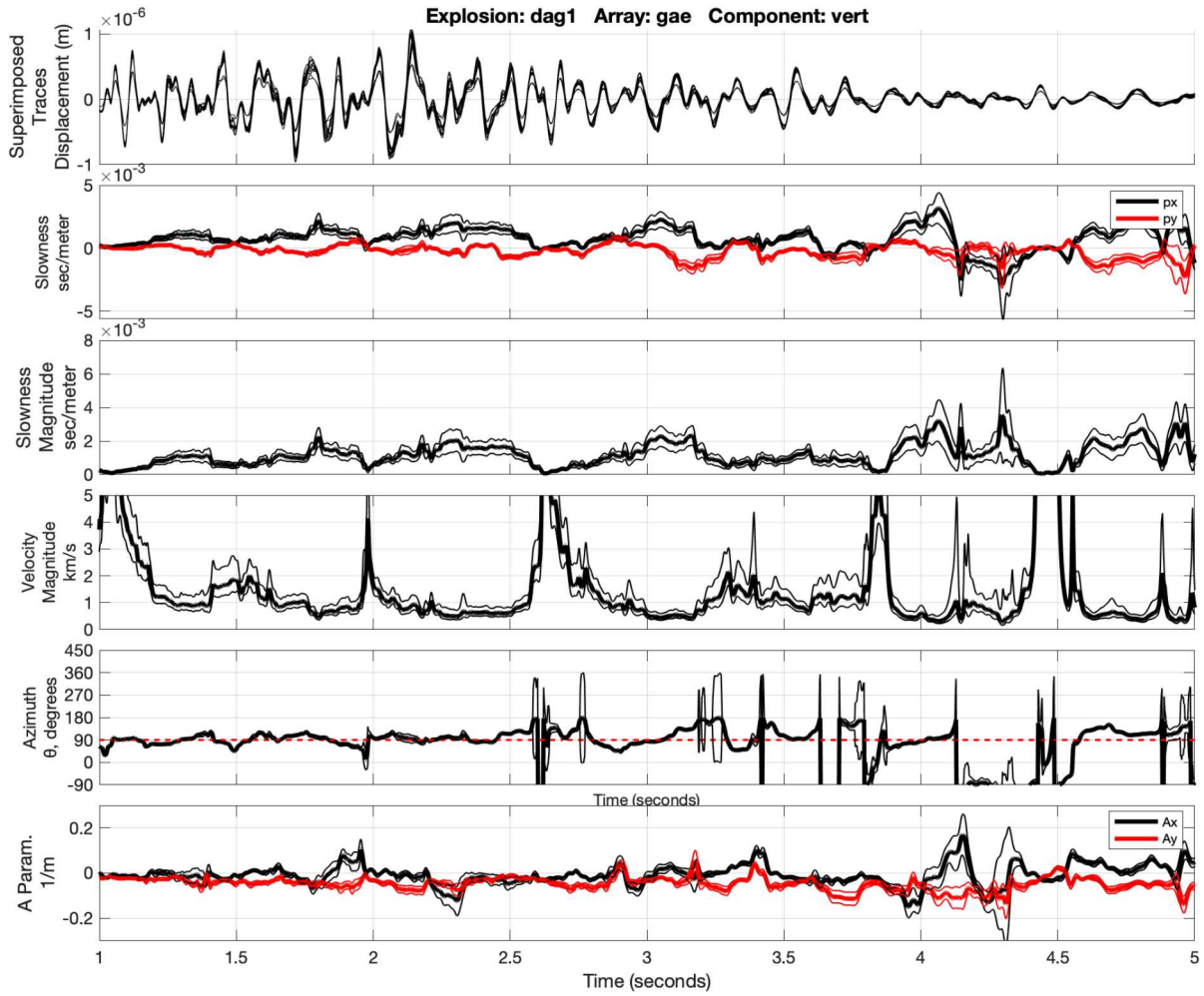

DAG 1 GAN gradiometer

Vertical component

In order from top to bottom:

1) Raw seismograms
2) Slowness in x and y direction
3) Slowness magnitude
4) Velocity magnitude
5) Azimuth of wave propagation (degrees from north)
6) Changes in radiation pattern, in x and y direction

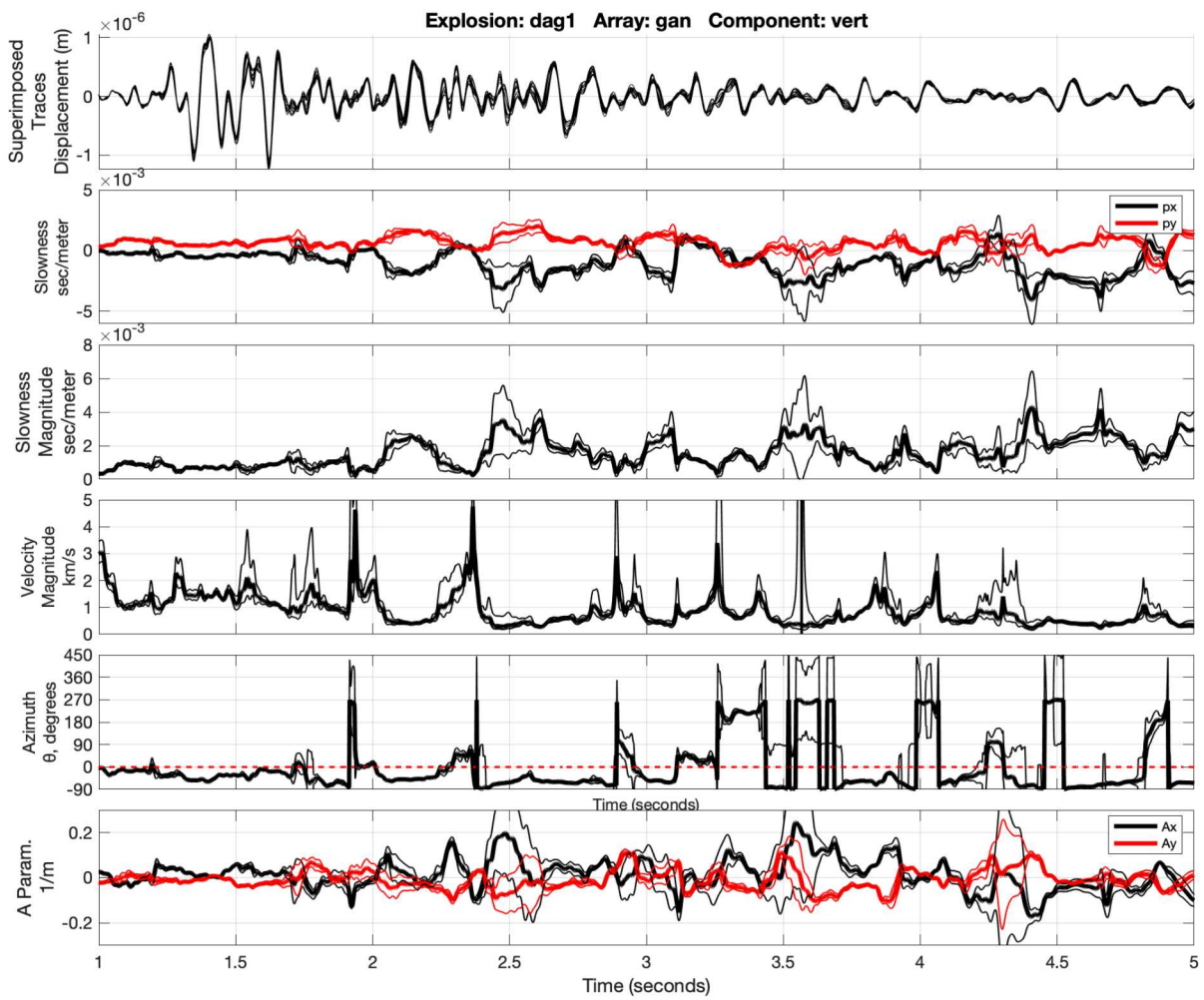

CWT: Displacement Data - Vertical Component

- Raw seismograms are qualitatively different
- Notable differences in time-frequency space
- Same explosion, different paths
- GAN array reaches highest power much later in time than GAE

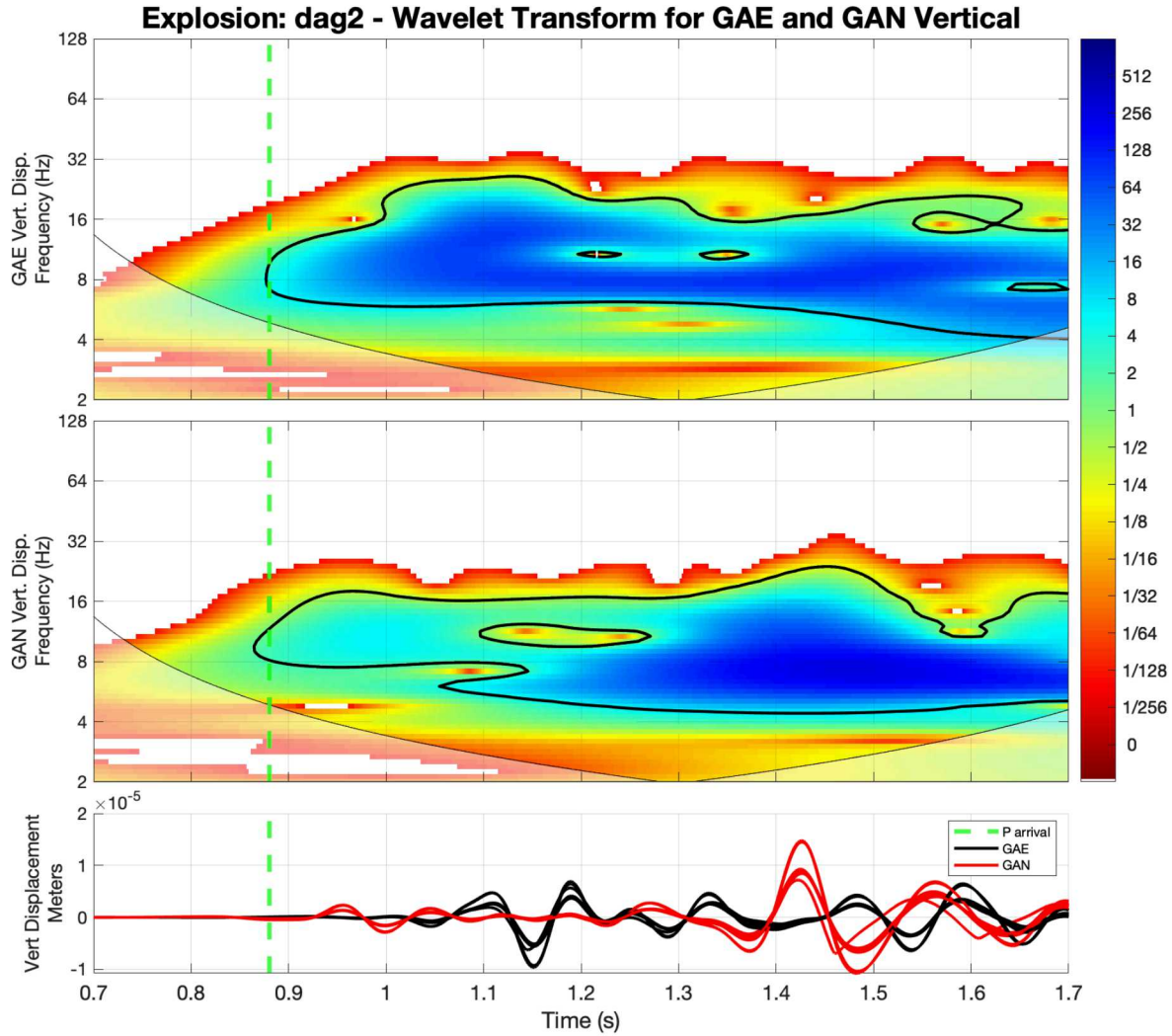

Wavelet Coherence: DAG1 displacement seismograms

- Broadly high coherence at low frequencies for vertical and transverse
- Vertical and radial components have several areas of high coherence at high frequencies (>= 10 Hz), including after P-wave arrival P-wave arrivals are 180^{o} out of phase (radial and vertical), arrow points left
  - We would expect them to be only ~90^{o} out of phase
- Areas of high coherence are not consistent between the components (radial, transverse, vertical)

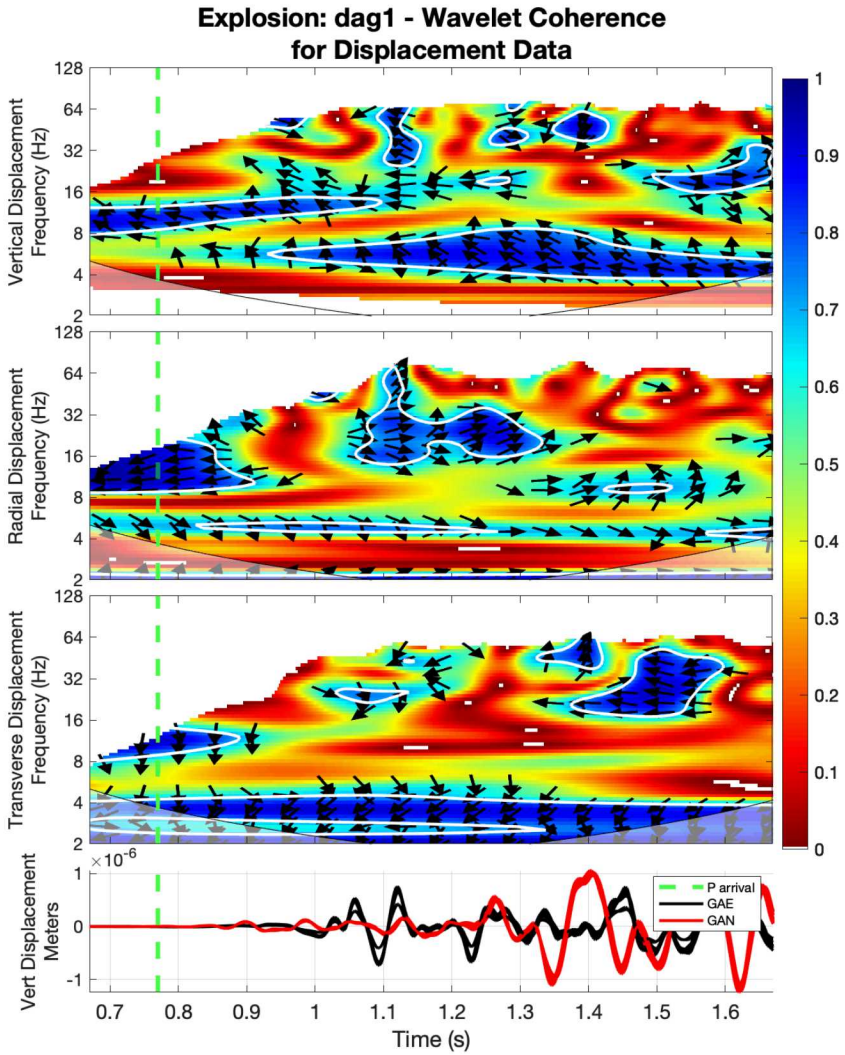

Wavelet Coherence: DAG2 displacement seismograms

- Highly coherent on lower frequencies < 4 Hz, almost completely non coherent at higher frequencies except for 10-15 Hz.
- Rolls over sharply below 4 Hz
  - Expected due to instrument response
- Relative phase between arrays changes are smooth and consistent within 95% confidence contour (white)
- Areas of high coherence are not consistent between the components (radial, transverse, vertical)

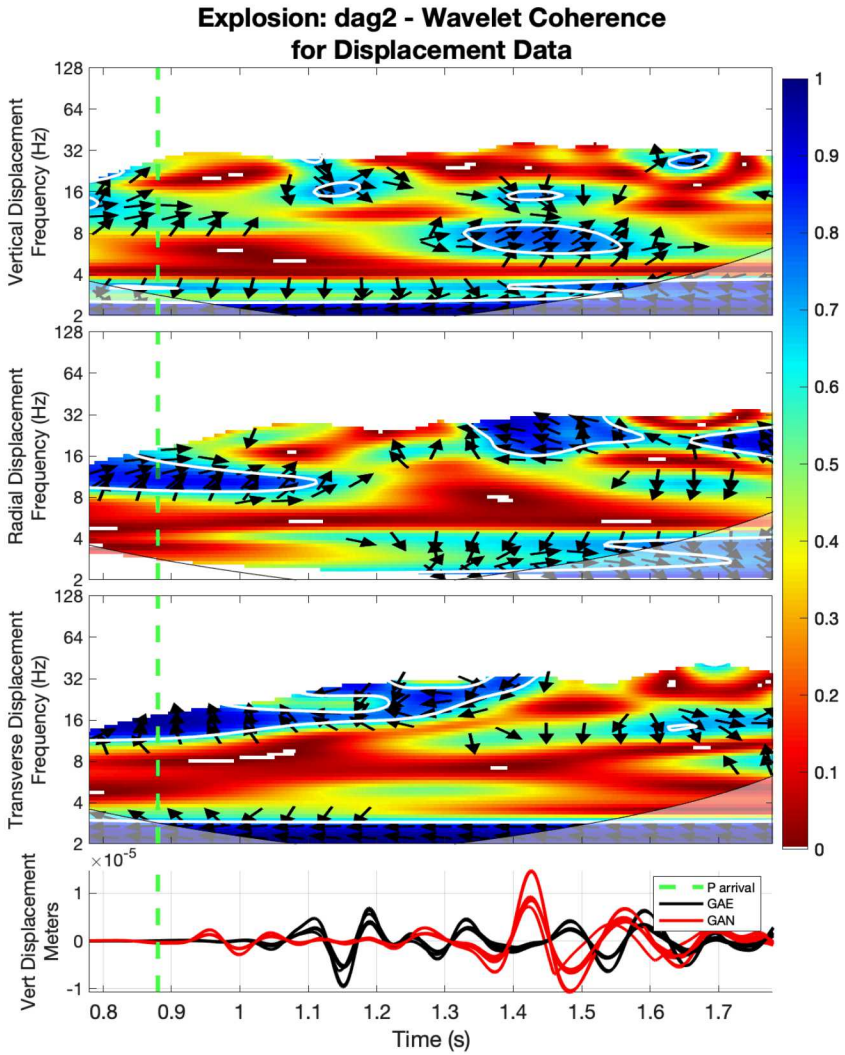

Wavelet Coherence: DAG3 displacement seismograms

- Broadly high coherence at low frequencies for all components
- Broadly low coherence at higher frequencies for all components, some high coherence for transverse later in figure
- P-wave arrivals are in phase (radial and vertical), arrow points right
  - we'd expect them to be 90 degrees out of phase
- Areas of high coherence are not consistent between the components (radial, transverse, vertical)

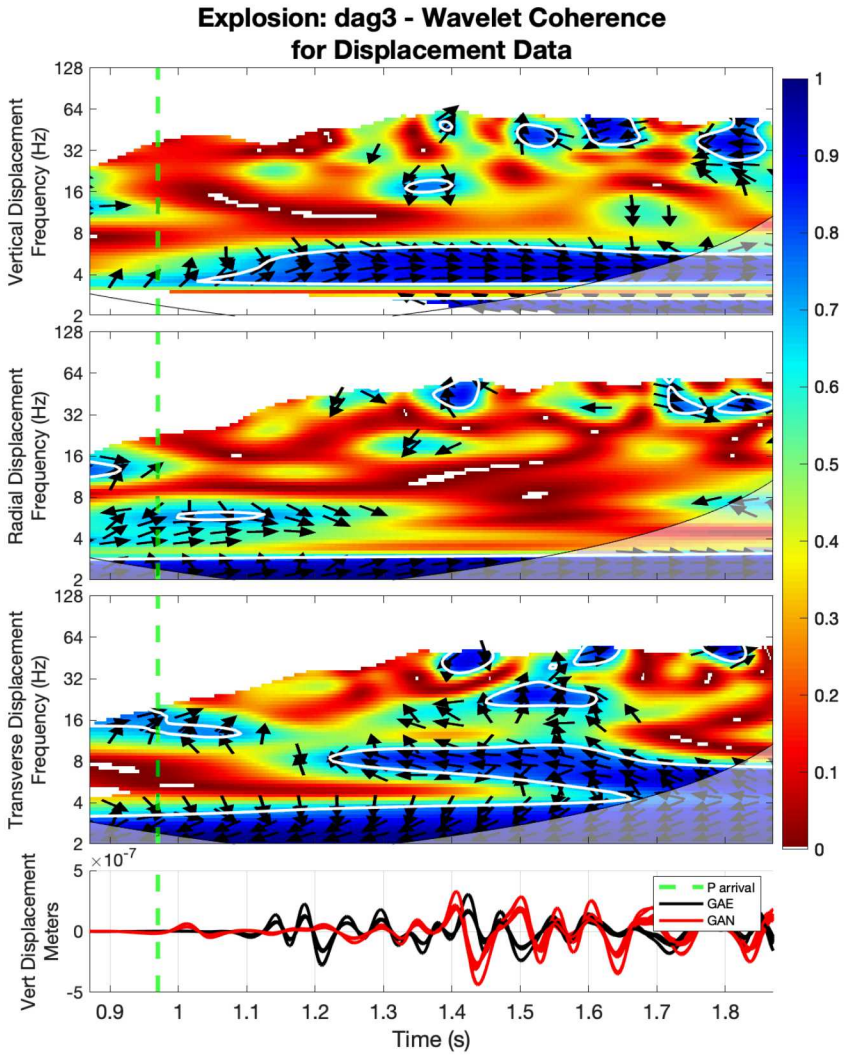

Wavelet Coherence: DAG1 Rotational motions

- Generally low coherence immediately post P arrival
- Transverse component has broad high coherence above about 12 Hz
- No consistent pattern between the 3 rotation components

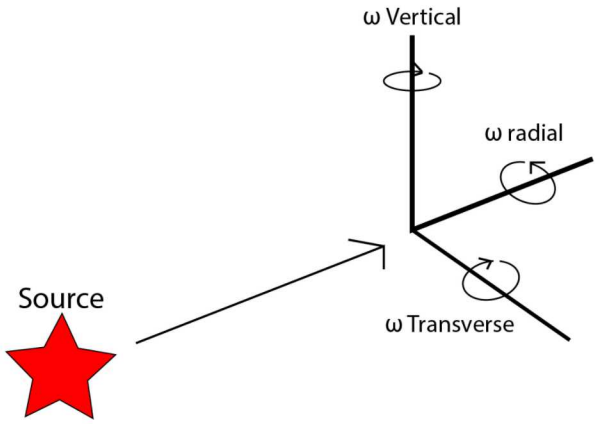

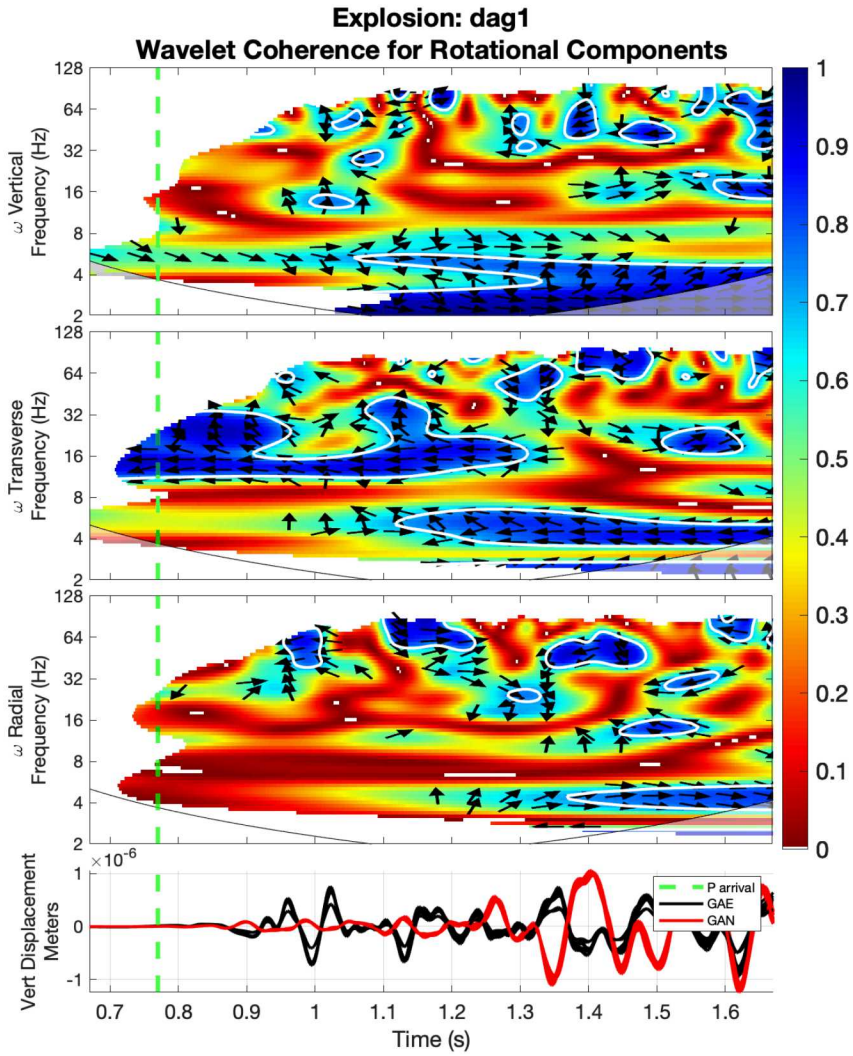

Wavelet Coherence: DAG2 Rotational motions

- Low coherence dominates the time-frequency space immediately post P arrival.
- Areas of high coherence have consistent, smoothly changing phase.
- Transverse component has higher coherence than radial or vertical components.

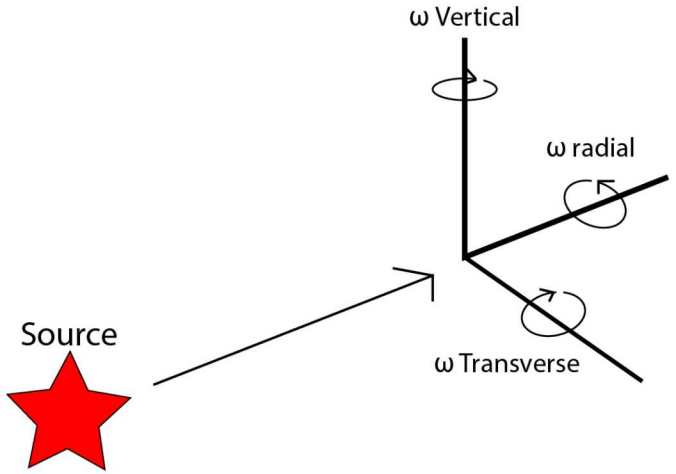

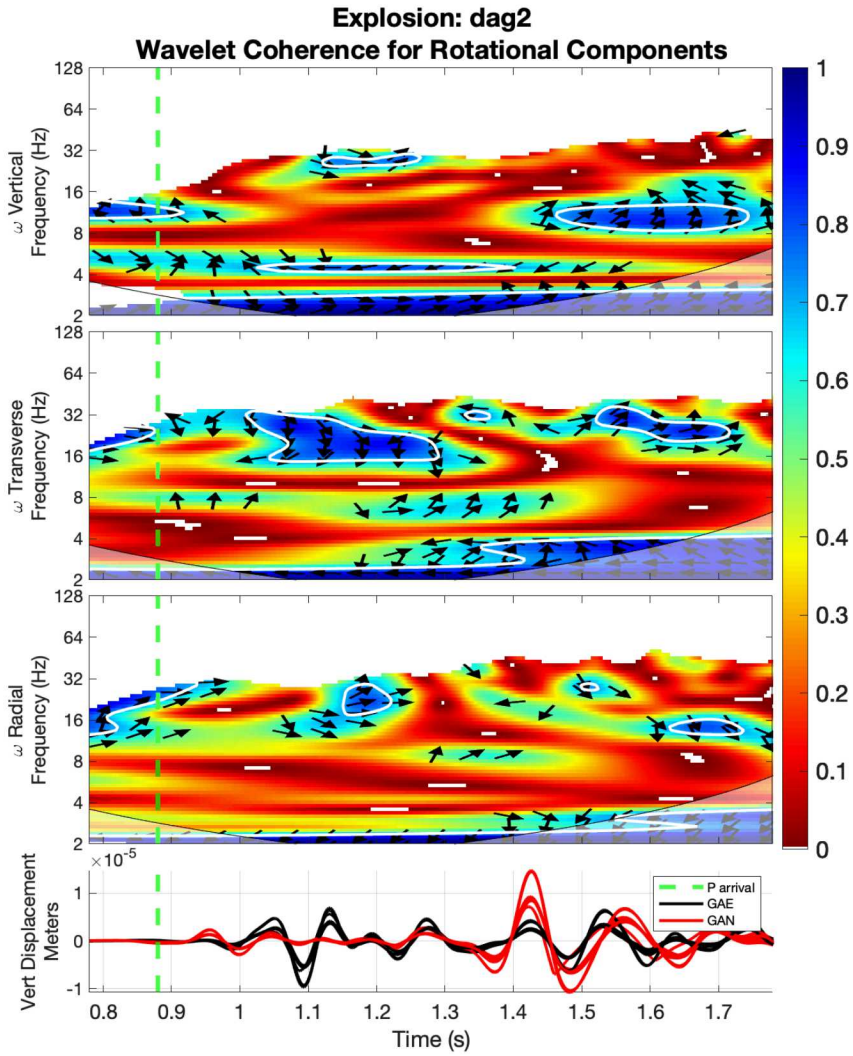

Wavelet Coherence: DAG3 Rotational motions

- Generally low coherence immediately post P arrival
- Radial component has broad region of high coherence below about 6 Hz
- No consistent pattern between the 3 rotational components

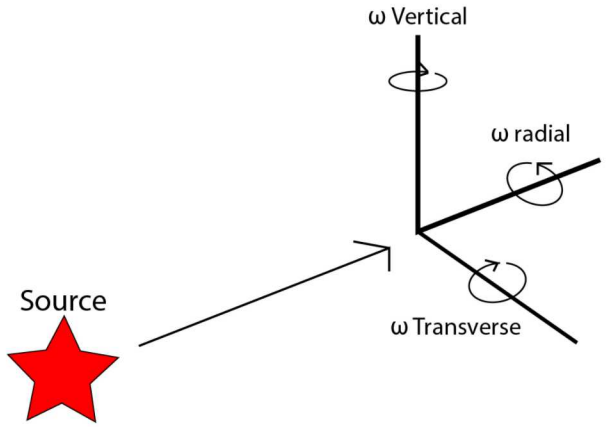

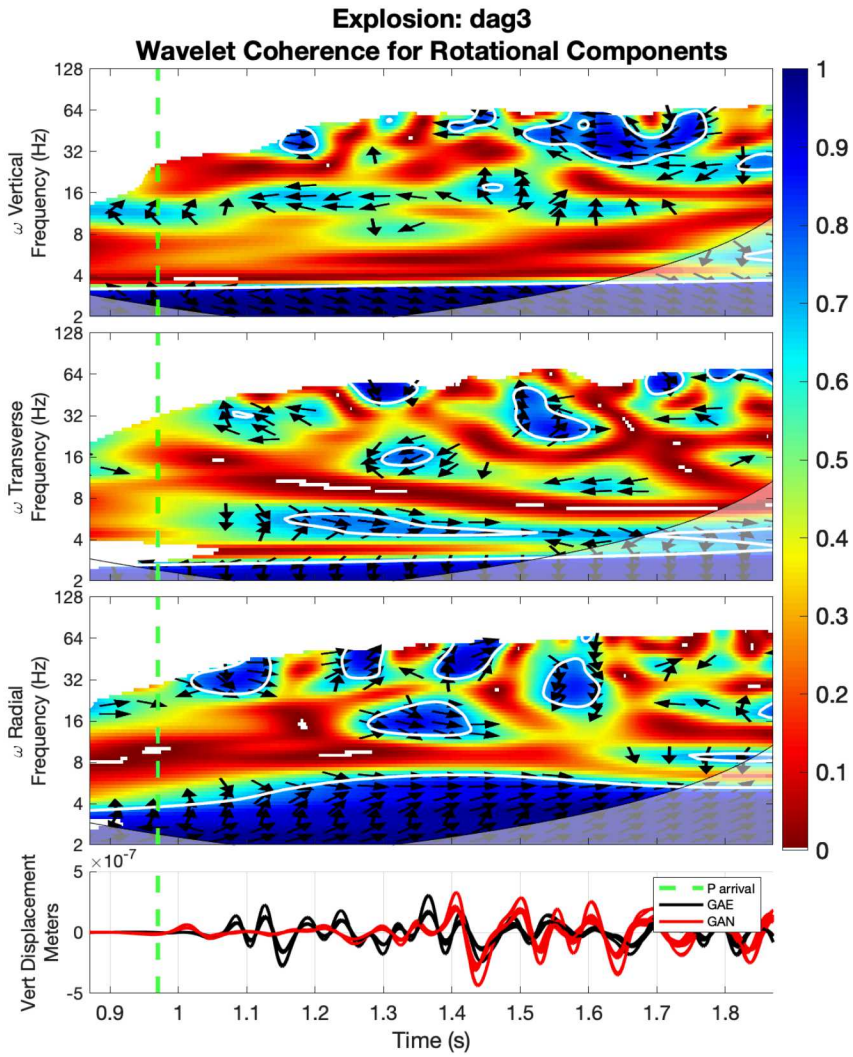

Envelope Decay – DAG 2

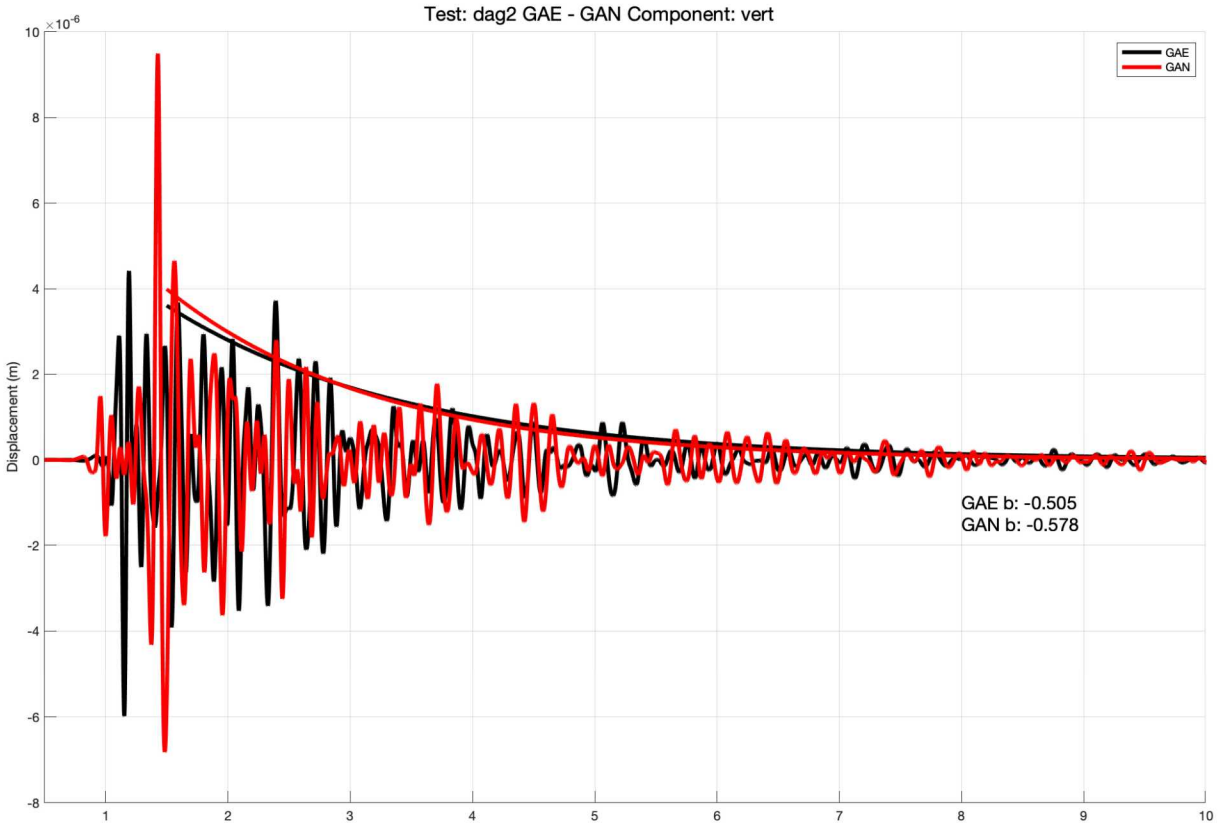

Discussion – Interpretations of Coherence

- Each explosion had a different yield and a different depth of burial
  - We don't expect each analysis to look similar from one explosion to another
- Coherence plots varied between:
  - Different rotational components: ω_r, ω_t, and ω_z
  - Different seismogram components: radial, transverse, and vertical

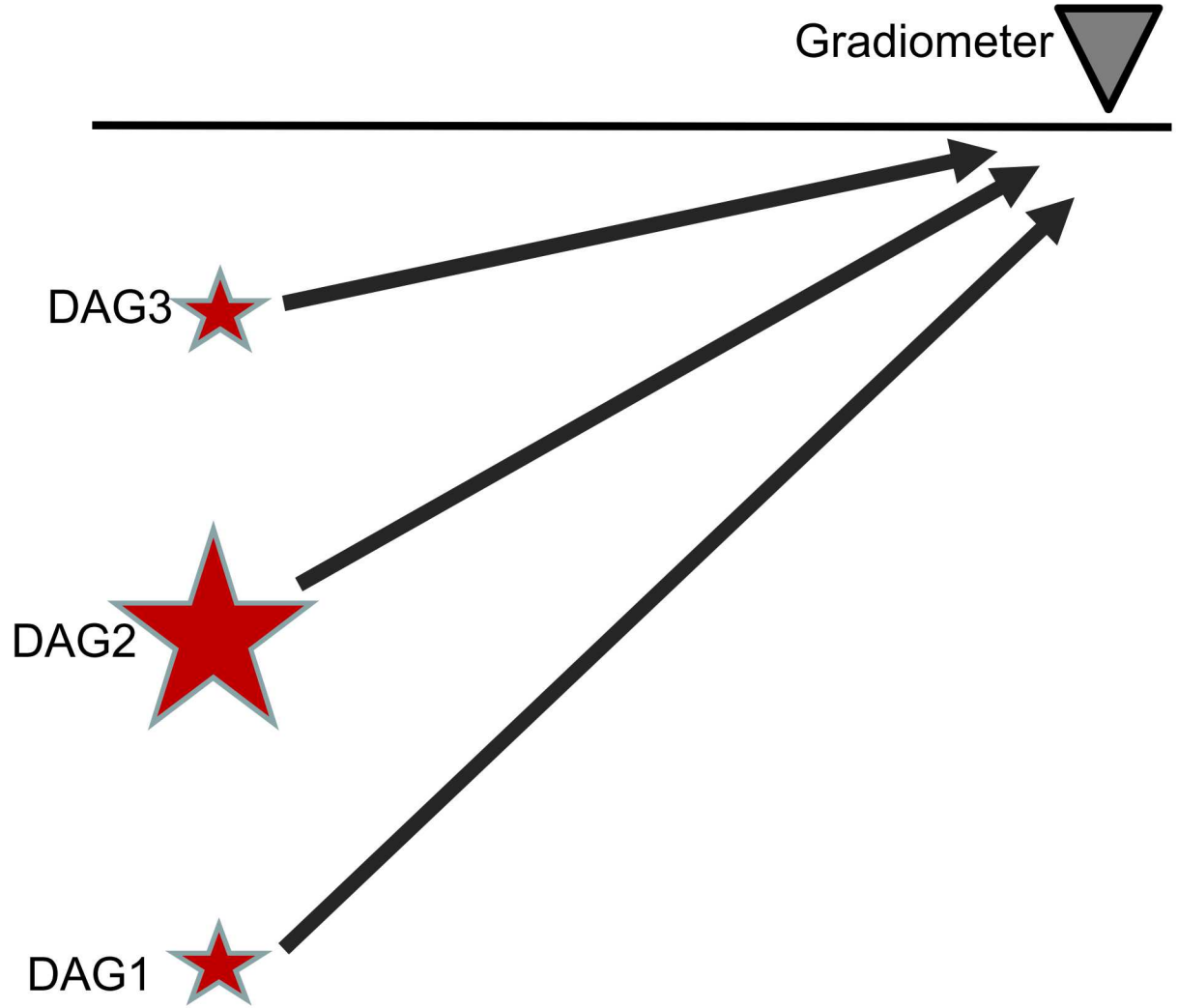

Discussion – Interpretations of Coherence (cont)

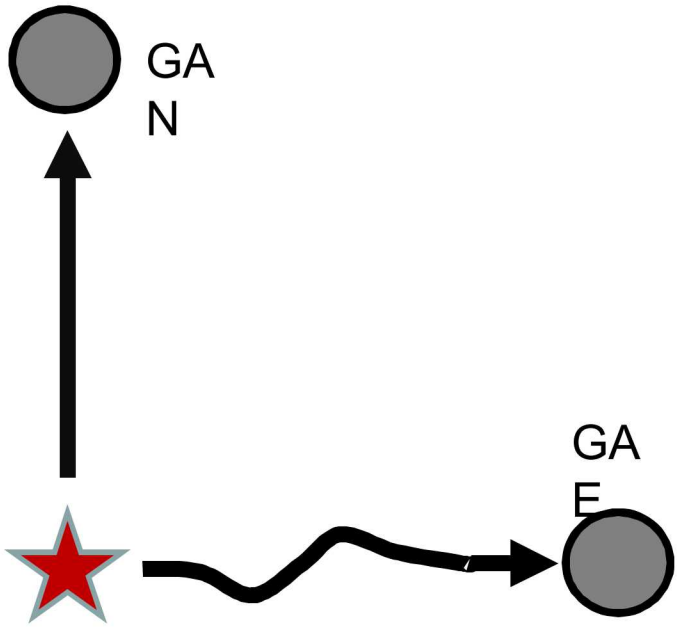

- Low coherence between GAE and GAN datasets
  - Suggests that the travel path significantly and measurably decorrelates the wavefield for the same travel distance.
  - lots of scattering - depends on azimuth of propagation
- Small frequency bands of high coherence, but frequency and time varied
  - Displacement data and rotational data – no consistent pattern
  - Rotational coherence hasn't been studied extensively
  - Could be coincidental – parts of the wavefields will be coherent due to chance

Discussion – Interpretations of Coherence (cont)

- Low coherence immediately after the P arrival, with very few exceptions - attributed to scattering and path effects
- Low coherence between each explosion (not shown)
  - Demonstrates path effects from dip are visible
- Implications for computing explosion yield
  - Yield calculations typically assume an isotropic source AND propagation of energy is fairly uniform in all directions
  - Not necessarily a correct assumption - different source-receiver paths could result in different computed yields
  - Near source wavefield distortions can impact source type estimates and yield estimates

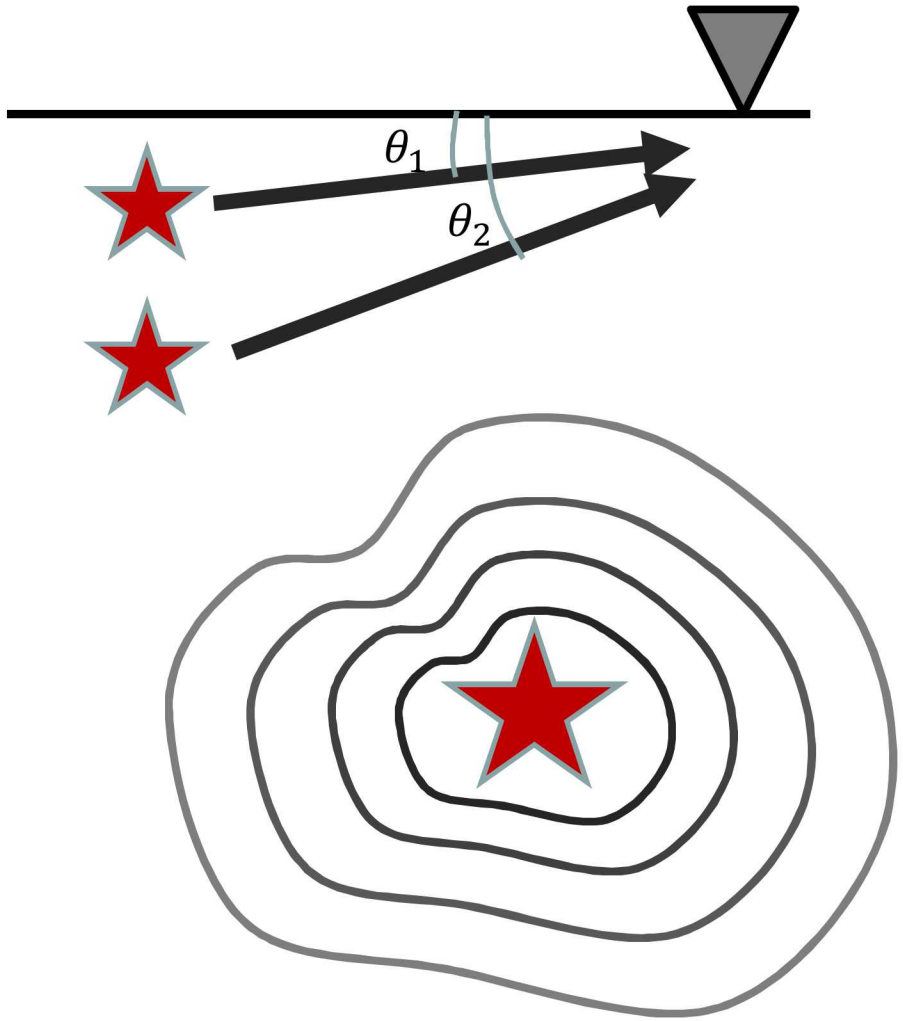

Discussion – Interpretations of Coherence (cont)

- Gradiometry might offer more insight into explosion characteristics for better quantification of yield
- Based on our observations, path effects can be substantial and must be accounted for to get accurate calculations
  - Includes azimuthal path effects and dip path effects

Future Work

- More gradiometers (not just two)
- Simultaneously deploy gradiometers with modern rotational seismometers for ground-truth comparison
- 3 Dimensional gradiometer (boreholes)
- Similar experiment in a variety of geologic settings

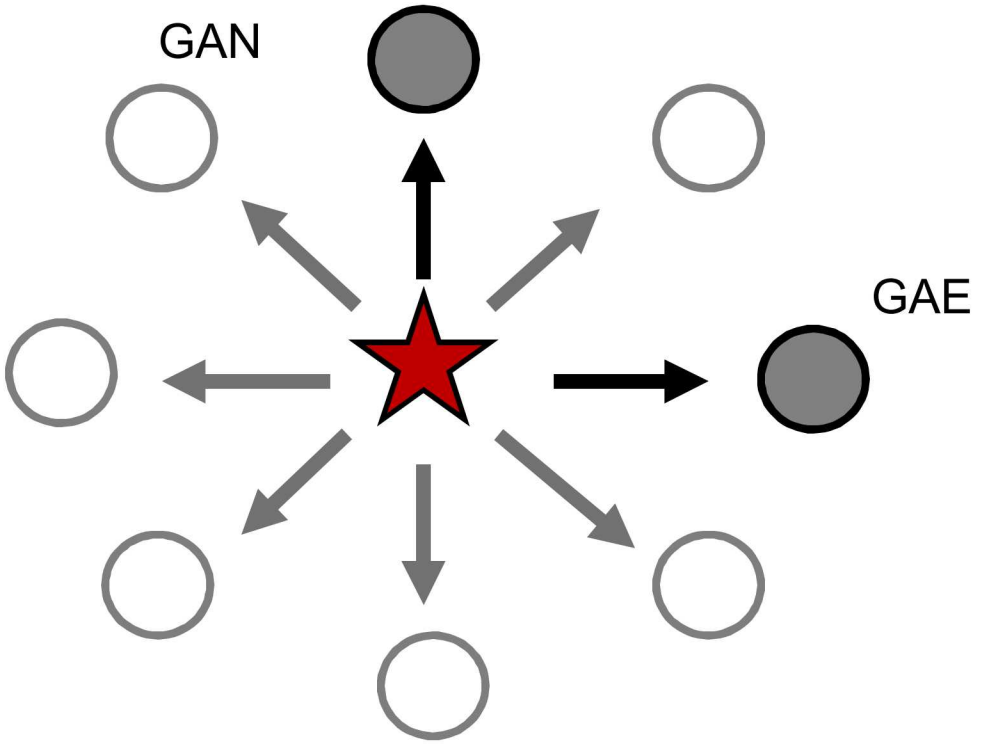

- Quantitatively measure the degree of scattering
- Additional analysis of envelope decay of the coda

References

Allmann, B. P., Shearer, P. M., & Hauksson, E. (2008). Spectral discrimination between quarry blasts and earthquakes in southern California. *Bulletin of the Seismological Society of America*, *98*(4), 2073–2079. https://doi.org/10.1785/0120070215

Aki, K., & Chouet, B. (1975). Origin of coda waves: Source, attenuation, and scattering effects. *Journal of Geophysical Research*, *80*(23), 3322–3342. https://doi.org/10.1029/JB080i023p03322

Bache, Thomas C. 1982.; Estimating the yield of underground nuclear explosions. *Bulletin of the Seismological Society of America* ; 72 (6B): S131–S168.

Cochard, A., Teisseyre, R., Takeo, M., & Majewski, E. (2006). Earthquake source asymmetry, structural media and rotation effects. *Earthquake Source Asymmetry, Structural Media and Rotation Effects*, 1–582. https://doi.org/10.1007/3-540-31337-0

Darrh, A., Poppeliers, C., & Preston, L. (2019). Azimuthally dependent seismic-wave coherence at the source physics experiment large-n array. *Bulletin of the Seismological Society of America*, *109*(5), 1935–1947. https://doi.org/10.1785/0120180296

Delouis, B., Charlety, J., & Vallée, M. (2009). A Method for Rapid Determination of Moment Magnitude Mw for Moderate to Large Earthquakes from the Near-Field Spectra of Strong-Motion Records (MWSYNTH). *Bulletin of the Seismological Society of America*, *99*(3), 1827–1840. https://doi.org/10.1785/0120080234

Gilman, D. L., Fuglister, F. J., & J. M. Mitchell, J. (1962). On the Power Spectrum of "Red Noise." *Journal of Atmospheric Sciences*, *20*.

Grinsted, A., Moore, J. C., & Jevrejeva, S. (2004). Application of the cross wavelet transform and wavelet coherence to geophysical time series. *Nonlinear Processes in Geophysics*, *11*(5/6), 561–566. https://doi.org/10.5194/npg-11-561-2004

Kisslinger, C., Koch, K., & Bowman, J. R. (1981). Procedures for Computing Focal Mechanisms from Local (SV/P)z Data. *Bulletin - Seismological Society of America*, *71*(6), 1719–1729.

Langston, C. A., & Liang, C. (2008). *Gradiometry for polarized seismic waves*. *113*(November 2007), 1–15. https://doi.org/10.1029/2007JB005486

Langston, C. A. (2007a). Wave gradiometry in two dimensions. *Bulletin of the Seismological Society of America*, *97*(2), 401–416. https://doi.org/10.1785/0120060138

Langston, C. A. (2007b). *Spatial Gradient Analysis for Linear Seismic Arrays*. *97*(1), 265–280. https://doi.org/10.1785/0120060100

Lee, W. H. K., Huang, B. S., Langston, C. A., Lin, C. J., Liu, C. C., Shin, T. C., Teng, T. L., & Wu, C. F. (2009). Progress in rotational ground-motion observations from explosions and local earthquakes in Taiwan. *Bulletin of the Seismological Society of America*, *99*(2 B), 958–967. https://doi.org/10.1785/0120080205

Liu, Cao, Chen, "Seismic Time-Frequency Analysis via Empirical Wavelet Transform", 2016;

Mellors, R. J., Pitarka, A., Matzel, E., Magana-Zook, S., Knapp, D., Walter, W. R., Chen, T., Snelson, C. M., & Abbott, R. E. (2018). The Source Physics Experiments large N array. *Seismological Research Letters*, *89*(5), 1618–1628. https://doi.org/10.1785/0220180072

Poppeliers, C., & Punoševac, P. (2013). Three-dimensional wave gradiometry for polarized seismic waves. *Bulletin of the Seismological Society of America*, *103*(4), 2161–2172. https://doi.org/10.1785/0120120165

Snelson, C. M., Bradley, C. R., Walter, W. R., Antoun, T., Abbott, R., Jones, K., Chipman, V. D., & Montoya, L. (2014). *The Source Physics Experiment (SPE) Science Plan*.

Sweetkind, D. S., & Drake II, R. M. (2007). Geologic Characterization of Young Alluvial Basin-Fill Deposits from Drill Hole Data in Yucca Flat, Nye County, Nevada. *Open-File Report*, 21. http://pubs.er.usgs.gov/publication/ofr20061390

Torrence, C., & Compo, G. P. (1997). A Practical Guide to Wavelet Analysis. *Bulletin of the American Meteorological Society*, *137*(2), 87–92.

Townsend, M., & Obi, C. (2015). *Data Release Report for Source Physics Experiments 2 and 3 (SPE-2 and SPE-3) Nevada National Security Site*. *3*(April), DOE/NV/25946--2282-REV 1. https://doi.org/10.2172/1179079

Townsend, M., L. B. Prothro, and C. Obi (2012). Geology of the Source Physics Experiment site, Climax Stock, Nevada Nation Security Site, Technical Report, National Security Technologies, Las Vegas, Nevada, 707 pp, DOE/NV/25946--1448.

Udías, Agustín; Raúl Madariaga, Elisa Buforn (2014). *Source Mechanisms of Earthquakes. Theory and Practice.* Cambridge University Press. 302 pp. Print. ISBN 978-1-107-04027-4.

Waldhauser, Felix; William L. Ellsworth. 2000. A Double-Difference Earthquake Location Algorithm: Method and Application to the Northern Hayward Fault, California. *Bulletin of the Seismological Society of America* ; 90 (6): 1353–1368. doi: https://doi.org/10.1785/0120000006

Wu, Y. M., & Zhao, L. (2006). Magnitude estimation using the first three seconds P-wave amplitude in earthquake early warning. *Geophysical Research Letters*, *33*(16), 4–7. https://doi.org/10.1029/2006GL026871

Zallishvili et al, "Spectral-Temporal Features of Seismic Loadings on the Basis of Strong Motion Wavelet Database", 2016.